Memorie della Società Astronomica Italiana

Supplementi - Vol. 1

Computational Astrophysics in Italy: Methods and Tools
Prima Riunione Nazionale

Bologna, 4-5 luglio 2002
Editor: Roberto Capuzzo Dolcetta

Visualization and computing tools

Astrophysical and cosmological supercomputing applications

Two selected topics of the round table on computational astrophysics in Italy: state and perspectives

Conclusions

Mem. S.A.It. Suppl. Vol. 1, 18
© SAIt 2003

Memorie della
Supplementi

A parallel implementation of a new fast algorithm for N-body simulations

P. Londrillo[1], C. Nipoti[2], and L. Ciotti[2]

[1] INAF – Osservatorio Astronomico di Bologna, via Ranzani 1, 40127 Bologna, Italy e-mail: `londrillo@bo.astro.it`

[2] Dipartimento di Astronomia, Università di Bologna, via Ranzani 1, 40127 Bologna, Italy e-mail: `nipoti@bo.astro.it, ciotti@bo.astro.it`

Abstract.
A new, momentum preserving fast Poisson solver for N-body systems sharing effective $O(N)$ computational complexity, has been recently developed by Dehnen (2000, 2002). We have implemented the proposed algorithms in a Fortran-90 code, and parallelized it by a domain decomposition using the MPI routines. The code has been applied to intensive numerical investigations of galaxy mergers, in particular focusing on the possible origin of some of the observed scaling relations of elliptical galaxies. We found that the Fundamental Plane is preserved by an equal mass merging hierarchy, while it is *not* in a scenario where galaxies grow by accretion of smaller stellar systems. In addition, both the Faber-Jackson and Kormendy relations are *not* reproduced by our simulations.

Key words. methods: N-body simulations – methods: numerical – galaxies: elliptical and lenticular, cD – galaxies: formation – galaxies: fundamental parameters

1. Introduction

In the last few years, fast algorithms for computing N-body interactions relying on the general multipole expansion techniques have been developed. These schemes, usually referred to as Fast Multipole Methods (FMMs, see, e.g., Greengard & Rokhlin 1987, 1997), are designed to have $O(N)$ computational complexity. However, it has been noted that only $O(N\log N)$ scaling is usually achieved in numerical implementation (see, e.g., Capuzzo-Dolcetta & Miocchi 1998, hereafter CM98). The $O(N\log N)$ operation count also characterizes the N-body codes based on tree algorithms, originally proposed by Barnes & Hut (1986, hereafter BH86). In addition, it has been shown by direct numerical tests that, for given accuracy, tree-codes are faster than the FMMs by a factor of ~ 4 (CM98). For this reason, most of the N-body codes currently used for astrophysical applications are based on

Send offprint requests to: P. Londrillo
Correspondence to: Osservatorio Astronomico di Bologna, via Ranzani 1, 40127 Bologna

the classical BH86 tree scheme, where the particle data are organized into a nested oct-tree cell structure. Interactions between distant particles are approximated by cell–particle interactions, and the distribution of the particles on each cell is represented by a multipole expansion, usually truncated to the quadrupole term.

Recently, a new scheme has been introduced (Dehnen 2000, 2002, hereafter D02), which can be seen as an original combination of the tree-based BH86 scheme and of the FMMs multipole expansion, truncated at a fixed low order level (the proposed $p = 3$ order results the optimal one). This scheme, implemented by the Author in a C++ code [named falcON, Force Algorithm with Complexity $O(N)$], results in a significant improvement over the existing BH86 tree-codes, in terms of uniform accuracy, linear momentum conservation, and CPU time performances. Moreover, the numerical tests presented in the D02 paper show that for an accuracy level $\epsilon \simeq 10^{-3}$, for the first time an *effective* $O(N)$ scaling in operation count, as predicted by the FMM theory, is in fact obtained. For these reasons two of us (P.L. and C.N.) have implemented this scheme in a new Fortran-90 code (FVFPS, a Fortran Version of a Fast Poisson Solver), and have then parallelized it by using the MPI procedures. A completion of the code to handle gas-dynamics using Euler equations and the AMR (Adaptive Mesh Refinement) techniques is under development. Here we briefly describe the main characteristics of Dehnen's algorithm, and we present our FVFPS implementation and its parallelization. The achieved accuracy level, the performances in terms of operation count speed-up, the effective $O(N)$ scaling, as well as the parallel scaling with the processors number, are then documented in numerical tests. Finally, we describe some interesting astrophysical applications of the code, in the context of the study of galaxy merging. Our version of the code is available upon request.

2. Dehnen's scheme

In the FMM approach, a system of particles is first organized in a oct-tree structure of nested cells, providing a hierarchical grouping of particles. For each pair of distant cells (A, B), the interactions between particles are then approximated by a Taylor expansion of the two-point Green function around the *geometrical center* of each cell by using spherical harmonics. In these cell-cell interactions the two-body symmetry of the exact Green function is preserved by the multipole approximation. In principle, a FMM-based scheme can achieve a prescribed accuracy ϵ by increasing the order p of the Taylor polynomial, and/or by lowering the expansion parameter $\eta \equiv r/R$ (where R is the distance between the two cell centers and r gives the typical size of a cell enclosing a particle group). Even if a formal, asymptotic scaling $O(N)$ is expected, the proposed algorithms in the original formulation (Greengard & Rokhlin, 1997) appear in fact to be less performing and of difficult application. Therefore, a first variant has been introduced in CM98, where the expansion order is kept fixed to $p = 2$, and only the η parameter controls the accuracy of the Taylor expansion. This approach takes advantage of the adaptivity of tree algorithms to select the pairs of cells (even belonging to different levels of refinements), which satisfy the opening criterium $r_{\rm crit}/R \le \theta$, where θ is a preassigned control parameter. To improve the efficiency of the scheme, a new definition of the critical size $r_{\rm crit}(A, B)$, has been also introduced. However, even in this improved formulation, the FMM scheme results to be not competitive with the classical BH86 tree-code.

Dehnen's scheme basically develops along similar lines, but with some new ingredients, which in fact succeeded to improve the overall efficiency in a substantial way:

- the Taylor polynomial expansion is performed in Cartesian components, and the expansion centers are the center of

mass of each cell, as in the BH86 tree-code;
- a fixed expansion order $p = 3$ is chosen as optimal;
- a new definition of the critical radius $r_{\rm crit}$ is introduced for each cell, to optimize the adaptive selection of all pairs of well-separated cells;
- a new, mass dependent control parameter $\theta = \theta(M)$ has been introduced, that assures faster performances and a more uniform error distribution. The $\theta(M)$ function is given in implicit form by

$$\frac{\theta^5}{(1-\theta)^2} = \frac{\theta^5_{\rm min}}{(1-\theta_{\rm min})^2}\left(\frac{M}{M_{\rm tot}}\right)^{-\frac{1}{3}}, \tag{1}$$

where $\theta_{\rm min}$ (the minimum value of θ, associated with the total mass) enters as a new, preassigned control parameter, and where M is the total mass enclosed in a cell.

The resulting force solver is then organized as follows:

(a) As in the BH86 code, an oct-tree structure of nested cells containing particles is first constructed. A generic cell A, when acting as a gravity "source" is characterized by the position of its center of mass $\mathbf{X}_A$, by its critical size r_A, mass M_A, and by the quadrupole tensor Q_A. For the same cell A, when acting as a gravity "sink" a set of (twenty) Taylor coefficients C_A are used to store the potential and acceleration values at $\mathbf{X}_A$.

(b) To compute these coefficients, a new procedure for the tree exploration has been designed: starting from the root cell, all pairs of cells (A, B) satisfying the acceptance condition $(r_A+r_B)/R \leq \theta$, are looked for in a sequential way. When the condition is satisfied, each cell of the selected pair accumulates the resulting interaction contributions in $C_A(B)$ or $C_B(A)$. In case of nearby cells (not satisfying the acceptance condition), the bigger cell of the pair is splitted, and the new set of pairs are then considered. However, in order to avoid visiting the tree too deeply, some empirical conditions are adopted to truncate the sequence, by computing directly (exact) two-body forces for particles in the smallest cells. The Author, by using a stack structure to order the visited cell-pairs, has introduced a powerful and efficient new algorithm able to perform this *interaction phase* in the force computations.

(c) Finally, once all the cell-cell interactions has been computed and stored in the C_A array, a final step is needed to evaluate the gravitational potential and the accelerations of the particles in the (generic) cell A. This *evaluation phase* can be performed by a simple and fast $O(N)$ tree-traversal.

In our F-90 implementation of the scheme above, we followed rather closely the algorithms as described in D02: at this stage of development and testing, we have neither attempted to optimize our implementation, nor to look for particular tricks to save computational time.

To parallelize the force solver, we have adopted a straightforward strategy, by first decomposing the physical domain into a set of non-overlapping subdomains, each containing a similar number of particles (a few per cent of tolerance is allowed). The set of particles on each subdomain, S_k, is then assigned to a specific processing unit, P_k. Each processor builds its own tree [step (a)], and computes the interaction phase for all the particles in its subdomain [step (b)]. Steps (a) and (b) are executed in parallel. By ordering the processors in a one-dimensional periodic chain, it is then possible to exchange (particles and tree-nodes) data between them, by a "send_receive″ MPI routine, in such a way that each processor can compute the interaction phase with the other subdomains. This phase is then performed by the following computational steps:

(i) The P_k processor sends its source-data to P_{k+s} and receives from the P_{k-s} a copy of its source-data, where $s = 1, 2, ...N_{\rm PE}/2$, and $N_{\rm PE}$ is the total number of processors.

(ii) At any given level s, each P_k computes, again in parallel, the interaction phase with particles and cells of P_{k-s}. Mutuality of the interactions allows to evaluate, at the same time, the results of these interactions for cells and particles of processor P_{k-s} to be stored as sink-data.

(*iii*) These accumulated sink-data (acceleration for particles and Taylor's coefficients for cells) are sent back to the P_{k-s} processor, while the corresponding sink-data of the P_k processor are received from processor P_{k+s} and added to the current P_k values. In this way, it is evident that by repeating step (*ii*) $N_{\rm PE}/2$ times and step (*iii*) $N_{\rm PE}/2-1$ times, the interactions of P_k particles with all other particles in the domain are recovered.

(*iv*) The final evaluation phase [step (c)], being fully local, is performed in parallel.

Besides the force solver, the N-body code has been completed by a leap-frog time integrator scheme, with a (uniform) time step size Δt determined adaptively using a local stability condition $\Delta t < 1/\sqrt{4\pi G\rho_{\rm max}}$, where G is the gravitational constant, and $\rho_{\rm max}$ the maximum of particle density. For typical simulations involving galaxy mergers, this adaptive (in time) step size keeps comparable to the value $T_{\rm dyn}/100$, where $T_{\rm dyn}$ represents a macroscopic dynamical time scale, and assures energy conservation with relative errors smaller than 0.1%.

3. Performances of the FVFPS code

We ran some test simulations in order to estimate the performances of our FVFPS code, and to compare it both with falcON and with the BH86 tree-code. We focus first on the analysis of the time efficiency in force calculation, considering (one–processor) *scalar simulations* of the N-body system representing a galaxy group, where each galaxy is initialized by a Hernquist (1990, hereafter H90) galaxy model. Values of the total number of particles N up to 2×10^6 are considered. The opening parameter given in eq. (1) is used by adopting $\theta_{\rm min}=0.5$, while for the BH86 code we used $\theta=0.8$: this choice results in comparable accuracies in the force evaluation. We ran our simulations on a Pentium III/1.133 GHz PC. For falcON and for the BH86 code we refer to the data published by D02, who used a Pentium III/933 MHz PC.

In Fig. 1 (left panel) we plot the time efficiency of the codes as a function of the number of particles; it is apparent from the diagram that FVFPS (solid line), as well as falcON (dashed line), reaches an effective $O(N)$ scaling, for $N \gtrsim 10^4$. Our F-90 implementation results to be slower than the C++ version by a factor of ~ 1.5: we think that this discrepancy may be due to differences in the details of the implementation, and also reflects a better intrinsic efficiency of the C++ with respect to the F-90 for this kind of algorithms (especially for routines where intensive memory accessing is required). In the same diagram the data relative to the BH86 tree-code are also plotted (dotted line), and the $O(N\log N)$ scaling is apparent. As already documented in D02, it is remarkable how, for fixed N and prescribed accuracy, the BH86 tree-code is significantly slower than the new scheme: for example for $N\simeq10^5$ the FVFPS code is faster by a factor of ~ 8. Therefore, even if the present F-90 implementation does no yet appear to be optimal, it gives further support to the efficiency of the D02 scheme, independently of the adopted programming language and of the implementation details.

The accuracy in force evaluation is documented on the right panel of Fig. 1, where we plot, as a function of N, the mean relative error on the acceleration modulus (filled circles)

$$\left\langle \frac{\Delta a}{a} \right\rangle \equiv \frac{1}{N}\sum_{i=1}^{N}\frac{|a^i_{\rm approx}-a^i_{\rm direct}|}{a^i_{\rm direct}}, \quad (2)$$

and the corresponding 99th percentile $(\Delta a/a)_9 9\%$ (empty squares), for FVFPS (solid lines) and, for comparison, in falcON (dashed lines). As usual, the reference acceleration values $a^i_{\rm direct}$ are evalu-

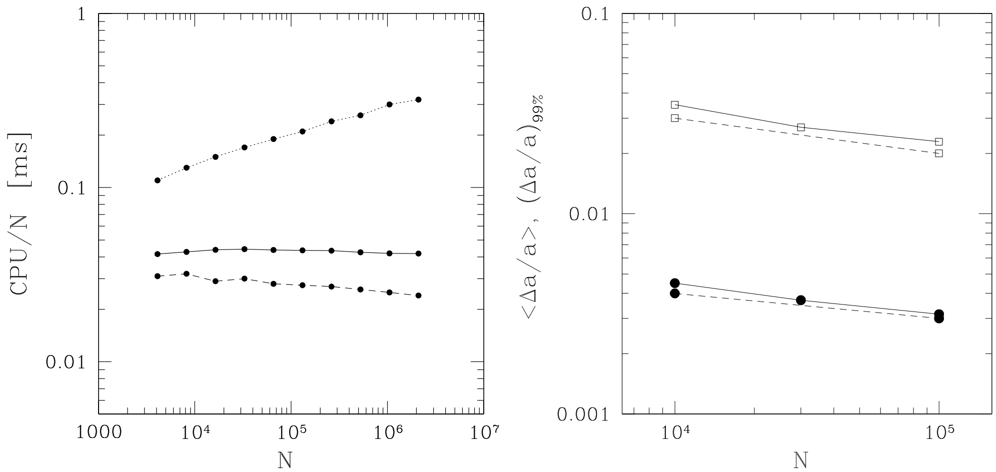

Fig. 1. *Left panel*: CPU time per particle as a function of total number of particles for BH86 tree-code (dotted line), falcON (dashed line; data from D02), and FVFPS (solid line). For the BH86 code $\theta = 0.8$, while in the last two cases $\theta = \theta(M)$, with $\theta_{\min} = 0.5$. *Right panel*: Mean error on the force calculation (filled circles) and the 99th percentile (empty squares), as a function of the number of particles in falcON (dashed line; data from D02), and in FVFPS (solid line).

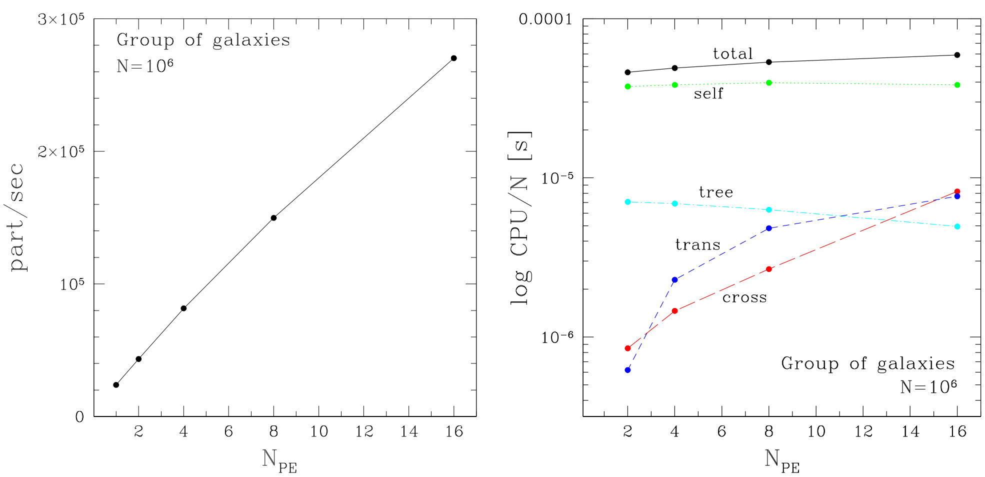

Fig. 2. *Left panel*: number of particle processed per second by the parallel version of the FVFPS code, as a function of the number of processors. The data refer to simulations of a group of galaxies with total number of particles $N = 1048576$. *Right panel*: CPU time per particle as a function of the number of processors for the same simulations in left panel. The different contributions are plotted (see text for an explanation).

ated by direct summation of the exact two-body Green function, while the approximated values are given with $\theta = \theta(M)$, and $\theta_{\rm min} = 0.5$. In this case, we have considered only simulations having a single H90 galaxy model. From the diagram it is apparent that, for both implementations, $\langle \Delta a/a \rangle$ and $(\Delta a/a)_9 9\%$ do not exceed a few 10^{-3} and a few per cent, respectively, assuring accuracies usually considered sufficient for astrophysical applications (see, e.g., CM98).

As outlined in the previous Section, we parallelized our code by using a domain decomposition with a load balancing essentially based only on particles number on each subdomain. This load balancing criterium seems in fact to work well, taking advantage of the intrinsic $O(N)$ scaling in the operation count of the basic scheme. In order to check the performance of the parallelized algorithm, we ran some simulations on the IBM Linux cluster (Pentium III/1.133 GHz PCs) at the CINECA center, in a range $N_{\rm PE} \leq 16$ in the number of processors. In this case the initial conditions are represented by a group of 8 one–component H90 galaxy models with a total number of particles $N = 1048576$. As can be observed in Fig. 2 (left panel), this parallelization is characterized by a rather well behaved linear scaling of the CPU time per particle versus $N_{\rm PE}$. This scaling can be better evaluated by considering the right panel of Fig. 2, where different contributions to the total CPU consumption are plotted. As expected, up to $N_{\rm PE} = 16$ the main contributions come by the tree building (“tree”) and by the the force computation in each sub-domain (“self”), corresponding to the step (i) and (ii), respectively, of the parallel scheme outlined in the previous Section. The contributions coming from the force evaluation among particles belonging to different subdomains (“cross”) and the cumulative time for all communication steps among processors (“trans”), which increase with $N_{\rm PE}$, keep smaller in the chosen range of parameters $(N, N_{\rm PE})$. Therefore, the $O(N)$ scaling of the base scheme, allows to estimate, for given N, the optimal configuration of the $N_{\rm PE}$ that can be used.

4. Simulations of galaxy merging

As an astrophysical application of the described FVFPS code, we consider here the study of the galaxy merging process. We checked the reliability of the numerical simulations performed with FVFPS for this kind of application (now time evolution is also considered), by running a few merging events, between spherically symmetric stellar systems, both with GADGET (Springel, Yoshida & White 2001), and with FVFPS. The results are in remarkable agreement: the remnants obtained with the two codes are practically indistinguishable for three-dimensional shape, circularized half–mass radius, circularized density and velocity dispersion profiles. As an illustrative example, in Fig. 3 we show the density profiles of the end–product of the merger obtained from the head–on parabolic encounter of two H90 models, with a total number of particles $N = 65536$ obtained with GADGET (empty symbols), and with FVFPS (filled symbols); note how also “minor” details, as the slope change in the density profile at $r \sim 10 r_{\rm M}$, are nicely reproduced. In addition, in both cases the change in total energy $\Delta E/E$ is smaller than 10^{-4} per dynamical time, over $100\, T_{\rm dyn}$. In this test, when using the FVFPS code, we adopted softening parameter $\varepsilon = 0.05$, initial time step $\Delta t = 0.01$, and (constant) $\theta = 0.65$; in the GADGET simulation we used $\varepsilon = 0.05$, $\alpha_{\rm tol} = 0.05$, $\Delta t_{\rm min} = 0$, $\Delta t_{\rm max} = 0.03$, $\alpha = 0.02$ (see Springel et al. 2001 for details), where the softening parameters and the time step parameters are in units of the galaxy core radius and dynamical time, respectively.

On the basis of the results of these tests, we used our N-body code to investigate with numerical simulations the effects of hierarchies of *dissipationless* galaxy mergers on the scaling relations of elliptical galaxies. This study is described in details in

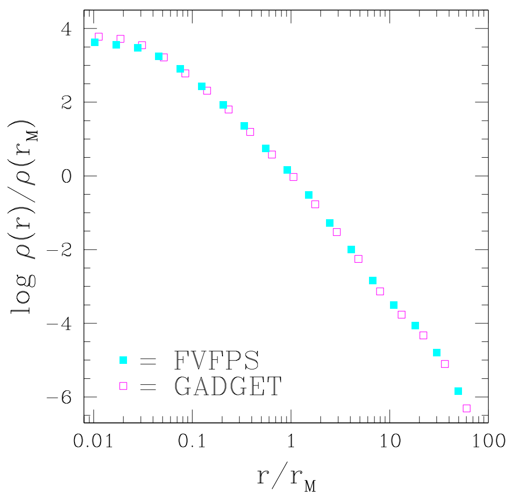

Fig. 3. Angle–average density profile of the remnant of the merging of two identical H90 galaxy models with FVFPS (full symbols), and with GADGET (empty symbols). $r_{\rm M}$ is the half–mass radius.

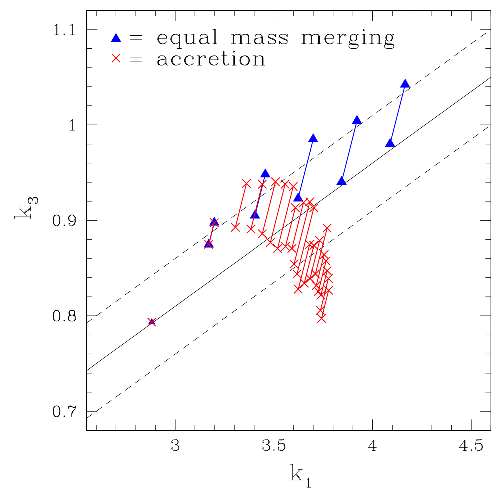

Fig. 4. The merging end–products in the (k_1, k_3) plane, where the solid line represents the edge–on FP relation with its observed 1-σ dispersion (dashed lines). Equal mass mergers are shown as triangles; crosses represent the accretion hierarchy. Bars show the amount of projection effects.

Nipoti, Londrillo & Ciotti (2002, hereafter NLC02). Here we report, as an example, the results relative to the effects of merging on the Fundamental Plane of elliptical galaxies (hereafter FP; Djorgovski & Davis 1987, Dressler et al. 1987). We considered a hierarchy of 5 equal mass mergers and a hierarchy of 19 accretion events, corresponding to an *effective* mass increase of a factor of $\sim$ 24 and $\sim$ 16, respectively: in the former case the successive generations are produced by merging pairs of identical systems obtained by duplicating the end–product of the previous step, while in the latter case each end–product merges with a seed galaxy. Each merging is produced in a head–on parabolic encounter. The seed galaxies are spherically symmetric one–component H90 galaxy models, with number of particles $N = 16384$ each. As a consequence of the merging hierarchy, the number of particles in the simulations increases with the galaxy mass: in the last merging of equal mass systems and of the accretion scenario, the total number of particles involved is of the order of 5.2×10^5 and 3.2×10^5, respectively.

In Fig. 4 we plot the results of equal mass merging and accretion simulations in the plane (k_1, k_3), where the *observed* FP is seen almost edge–on, with best–fit $k_3 = 0.15k_1 + 0.36$ (solid line) and scatter $\mathrm{rms}(k_3) \simeq 0.05$ (dashed lines; see Bender, Burstein & Faber 1992). In the diagram the end–products of equal mass mergers and accretion are identified by triangles and crosses, respectively. The (common) progenitor of the merging hierarchies (point without bar) is placed on the edge–on FP. The straight lines in Fig. 4, associated with the merger remnants, represent the range spanned in the (k_1, k_3) space by each end–product, when observed over the solid angle, as a consequence of projection effects. It is interesting to note that for all the end–products the projection effects are of the same order as the observed FP dispersion. In addition it is also apparent from Fig. 4

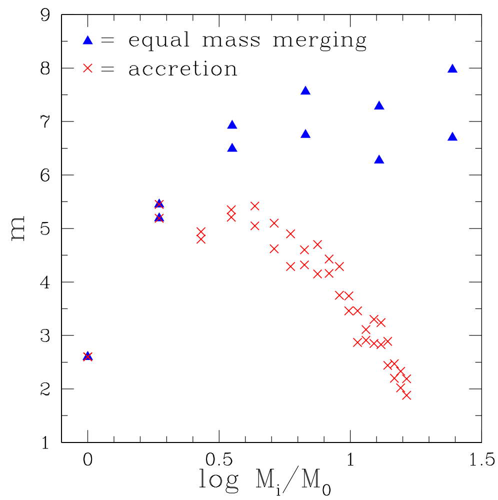

Fig. 5. Sersic best fit parameter m vs. total stellar mass of the end–products at stage i of the merging hierarchy. Symbols are the same as in Fig. 4

how, in case of equal mass merging, k_3 and k_1 increase with merging in a way full consistent with the observed FP tilt and thickness. On the other hand, in the case of accretions, after few steps the end–products are characterized by a k_3 *decreasing* for increasing k_1, at variance with the FP slope and the trend shown by the end–products of equal mass mergers. As a consequence, the last explored models (corresponding to an effective mass increase of a factor ~ 16) are found well outside the FP scatter.

The different behavior of the end–products in the two scenarios is due mainly to effects of *structural non–homology*. This is clearly shown by an analysis of the projected stellar mass density profiles of the end–products. In fact, we fitted (over the radial range $0.1 \lesssim R/\langle R\rangle_e \lesssim 4$) the projected density profiles of the end–products with the Sersic (1968) $R^{1/m}$ law, and in Fig. 5 we plot the best fit parameter m as a function of the total mass of the systems, for equal mass mergers (triangles) and accretion (crosses). Clearly, the best-fitting m depends on the relative orientation of the line–of–sight and of the end–products of the simulations: the two points for each value of the mass in Fig. 5 show the range of values spanned by m when projecting the final states along the shortest and longest axis of their inertia ellipsoids. In case of equal mass merging, the trend is m increasing with galaxy mass, as observed in real elliptical galaxies (see, e.g., Bertin, Ciotti & Del Principe 2002 and references therein). On the contrary, in case of accretion the best Sersic m parameter decreases at increasing mass of the end–product, a behavior opposite to what is empirically found.

As it is well known, elliptical galaxies follow, besides the FP, also other scaling relations, such as the Faber–Jackson (hereafter FJ, Faber & Jackson 1976), and the Kormendy (1977) relations. It is remarkable that, in our simulations, both the equal mass merging and the accretion hierarchies fail at reproducing these two relations. In fact, the end–products have central velocity dispersion lower, and effective radius larger than what predicted by the FJ and the Kormendy relations, respectively. In case of equal mass mergers, these two effects curiously compensate, thus preserving the edge–on FP. In other words, the remnants of *dissipationless* merging like those described, are *not* similar to real elliptical galaxies, though in some cases they reproduce the edge–on FP (see NLC02 for details).

5. Conclusions

The main results of our work can be summarized as follows:

- Our implementation of the D02 scheme in a F-90 N-body code (FVFPS) has effective $O(N)$ complexity for number of particles $N \gtrsim 10^4$, though its time efficiency is lower by a factor of ~ 1.5 than Dehnen's C++ implementation.
- As shown by numerical tests, the parallelized version of the FVFPS code has good scaling with the number of processors (for example for numbers of parti-

cles $N \simeq 10^6$, at least up to 16 processors).
- We found very good agreement between the results of merging simulations performed with our FVFPS code and with the GADGET code.
- From an astrophysical point of view, our high resolution simulations of hierarchies of *dissipationless* galaxy mergers indicate that *equal mass* merging is compatible with the existence of the FP relation. On the other hand, when an *accretion* scenario is considered, the merger remnants deviate significantly from the observed edge–on FP (see also NLC02).
- The different behavior with respect to the FP of the merger remnants in the two scenarios is a consequence of structural non–homology, as shown by the analysis of their projected stellar density profiles.
- In any case, the end–products of our simulations fail to reproduce both the FJ and Kormendy relations. In the case of equal mass merging, the combination of large effective radii and low central velocity dispersions maintains the remnants near the edge–on FP.

Acknowledgements. We would like to thank Walter Dehnen for helpful discussions and assistance. Computations have been performed at the CINECA center (Bologna) under the INAF financial support. L.C. was supported by MURST CoFin2000.

References

Barnes J. E., Hut P., 1986, Nature, 324, 446 (BH86)
Bender R., Burstein D., Faber S. M., 1992, ApJ, 399, 462
Bertin G., Ciotti L., Del Principe M., 2002, A&A, 386, 1491
Capuzzo-Dolcetta R., Miocchi P., 1998, Journal of Computational Physics, 143, 29 (CM98)
Dehnen W., 2000, ApJ, 536, L39
Dehnen W., 2002, Journal of Computational Physics, preprint (astro-ph/0202512), (D02)
Djorgovski S., Davis M., 1987, ApJ, 313, 59
Dressler A., Lynden-Bell D., Burstein D., Davies R.L., Faber S.M., Terlevich R., Wegner G., 1987, ApJ, 313, 42
Faber S.M., Jackson R.E., 1976, ApJ, 204, 668
Greengard L., Rokhlin V., 1987, Journal of Computational Physics, 73, 325
Greengard L., Rokhlin V., 1997, Acta Numerica, 6, 229
Hernquist L., 1990, ApJ, 356, 359 (H90)
Kormendy J., 1977, ApJ, 218, 333
Nipoti C., Londrillo P., Ciotti L., 2002, MNRAS, submitted (NLC02)
Sersic J.L., 1968, Atlas de galaxias australes. Observatorio Astronomico, Cordoba
Springel V., Yoshida N, White S.D.M., 2001, New Astronomy, 6, 79

Mem. S.A.It. Suppl. Vol. 1, 145

Memorie della
Supplementi

High-resolution re-simulations of massive DM halos and the Fundamental Plane of galaxy clusters

B. Lanzoni[1], A. Cappi[1], and L. Ciotti[2]

[1] INAF – Osservatorio Astronomico di Bologna, via Ranzani 1, 40127 Bologna, Italy e-mail: lanzoni@bo.astro.it, cappi@bo.astro.it

[2] Dipartimento di Astronomia, Università di Bologna, via Ranzani 1, 40127 Bologna, Italy e-mail: ciotti@bo.astro.it

Abstract. Pure N-body high-resolution re-simulations of 13 massive dark matter halos in a ΛCDM cosmology are presented. The resulting sample is used to investigate the physical origin of the Fundamental Plane, "Faber-Jackson", and "Kormendy" relations observed for nearby galaxy clusters. In particular, we focus on the role of dissipationless hierarchical merging in establishing or modifying these relations. Contrarily to what found in the case of the Faber-Jackson and Kormendy relations for *galaxies* (see Londrillo, Nipoti & Ciotti, this conference), dissipationless merging on *cluster scales* produces scaling relations remarkably similar to the observed ones. This suggests that gas dissipation plays a minor role in the formation of galaxy clusters, and the hierarchical merger scenario is not at odd with the observed regularity of these systems.

Key words. dark matter – galaxies: clusters: general

1. Introduction

Like early-type galaxies, also galaxy clusters follow well defined scaling relations among their main observables: in particular, a luminosity–velocity dispersion relation (i.e., a "Faber-Jackson–like" relation), a luminosity–radius relation (i.e., a "Kormendy–like" relation), and the Fundamental Plane (hereafter FP; e.g., Schaeffer et al. 1993, hereafter S93; Adami et al. 1998; and for ellipticals: Djorgovski et al. 1987; Dressler et al. 1987; Faber & Jackson 1976; Kormendy 1977). Besides their potential importance as distance indicators, these relations contain information on the cluster formation and evolution processes. Within the commonly accepted cosmological scenario, where cold dark matter (CDM) is the dominant component of the Universe, structure formation is driven by hierarchical dissipationless merging: small DM halos form first, then they merge to-

Send offprint requests to: B. Lanzoni
Correspondence to: Osservatorio Astronomico di Bologna,via Ranzani 1, 40127 Bologna

gether to form larger systems, and the evolution of the baryonic matter follows that of the hosting DM halos.

The importance of investigating the physical origin of the observed scaling relations, and the role of dissipationless hierarchical merging in establishing or modifying them, is therefore apparent, and explains the large number of theoretical works devoted to this problem in the case of elliptical galaxies (e.g. Capelato et al. 1995; Nipoti, Londrillo, Ciotti 2002a,b; Gonzales & van Albada 2002; Evstigneeva et al. 2002; Dantas et al. 2002; Londrillo et al., this conference). In particular, it has been shown that, while the FP is reproduced by the end–products of equal mass mergers, the Faber–Jackson and the Kormendy relations are *not* (Nipoti et al. 2002ab; Londrillo et al., this conference). In the case of galaxy clusters however, almost no theoretical studies are devoted to their FP (see, e.g., Pentericci, Ciotti & Renzini 1995; Fujita & Takahara 1999; Beisbart, Valdarnini & Buchert 2001).

We address this problem in the present work, by means of high resolution re-simulations of very massive DM halos (the hosts of galaxy clusters) in a ΛCDM cosmology. Following their hierarchical dissipationless evolution in detail, we verify whether they reproduce the observed scaling relations, both at the present time, and at higher redshift. A full analysis of this work will be given elsewhere (Lanzoni et al., in preparation), while we present here a selection of the main astrophysical results, focusing on the numerical issues.

2. High-resolution re-simulations

To investigate whether the dark matter counterpart of galaxy clusters, as obtained by numerical simulations, do define the observed scaling relations, a large enough sample of very massive DM halos was needed. For this purpose, we have employed the dissipationless "Very Large Simulations" (VLS; see Yoshida, Sheth, & Diaferio 2001), where the simulated comoving volume of the Universe is sufficiently large: the box side is of $479\,h^{-1}$Mpc, with $H_0 = 100\,h^{-1}$ km s^{-1} Mpc^{-1}, and $h = 0.7$. The adopted cosmological model is a ΛCDM Universe with $\Omega_{\rm m} = 0.3$, $\Omega_\Lambda = 0.7$, spectral shape $\Gamma = 0.21$, and normalization to the cluster local abundance, $\sigma_8 = 0.9$. The total number of particles is 512^3, of $6.86 \times 10^{10} M_\odot/h$ mass each.

From these simulations, we have selected a sample of 13 halos with masses between $10^{14} M_\odot/h$ and $2.3 \times 10^{15} M_\odot/h$. They span a variety of shapes, from nearly round to more elongated. The richness of their environment also changes from case to case, with the less isolated halos usually surrounded by pronounced filamentary structures, containing massive neighbors (up to 20% of their mass). All the selected halos are required to have a massive progenitor at redshift $z = 0.5$ (their masses range between 6×10^{13} and $1.5 \times 10^{15} M_\odot/h$), and also at $z = 1$ (with masses between 4×10^{13} and $7 \times 10^{14} M_\odot/h$). Such a choice allows us to study galaxy clusters not only locally, but also at higher redshift.

Given the mass resolution of the simulations, less than 1500 particles compose a halo of $10^{14} M_\odot/h$, and its properties entering the FP relation cannot be accurately determined. We have therefore resimulated at higher resolution the halos in our sample, by means of the technique introduced by Tormen, Bouchet & White (1997), that we briefly summarize in the following.

The first step is to select, in a given cosmological simulation, the halo one wants to reproduce at higher resolution. Then, all the particles composing the selected halo and its immediate surroundings are detected in the initial conditions of the parent simulation: the number of particles within the region thus defined is increased, and the region is therefore called "the high resolution (HR) region". As a consequence, the mean inter-particle separation decreases, and the corresponding high-frequency modes of the primordial fluctuation spectrum are added to those on larger scales originally used in the parent simulation. The overall displacement field is also modified consequently. At the same time, the distribution of surrounding particles is smoothed by means of a spherical grid, whose spacing increases with the distance from the center: in such a way, the original surrounding particles are replaced with a smaller number of *macroparticles*, whose mass grows with the distance from the HR region. Thank to this method, even if the number of particles in the HR region is increased, the total number of particles to be evolved in the simulation remains small enough to require reasonable computational costs, while the tidal field that the overall particle distribution exerts on the HR region remains very close to the original one. For the new initial configuration thus produced, vacuum boundary conditions are adopted, i.e., we assume a vanishing density fluctuation field outside the spherical distribution of particles with diameter equal to the original box size L. A new N-body simulation is then run starting from these new initial conditions, and allows to re-obtain the selected halo at the suited resolution.

We have applied this technique to the 13 massive DM halos selected in the VLS. For 8 out of the 13 selected halos, the resolution has been increased by a factor ~ 33, using high-resolution particles of $\sim 2.07 \times 10^9 M_\odot/h$ each, while a factor of 2 improvement has been adopted for the 5 intermediate mass halos (the particle mass is $10^9 M_\odot/h$ in this case). The gravitational softening used for the high-resolution region is $\epsilon = 5\,\mathrm{kpc}/h$, corresponding to about 0.2% and 0.5% of the virial radius of most and less massive halos, respectively. This scale length represents the spatial resolution of the resimulations, to be compared with that of $30\,\mathrm{kpc}/h$ of the original VLS. Note that to prevent low-resolution macroparticles to "contaminate" the final resimulated halo (i.e., to end within its virial radius), we need to define the HR region not only through the particles of the halo itself in the parent simulation, but considering also a boundary region in its immediate surroundings. This is particularly important in the case of less massive halos, since the small number of their composing particles does not allow to define their encompassing region in the initial conditions with enough precision. To avoid such a "contamination" problem in our re-simulations, a radius of about $3\,r_{\rm vir}$ and $5\,r_{\rm vir}$ for the boundary region was necessary for the most and the less massive halos, respectively. The resulting number of high and low resolution particles are listed in Table 1, together with their sum[1]. To run the resimulations, the parallel dissipationless tree-code "GADGET" (Springel, Yoshida & White 2001) has been used on the IBM SP2 and SP3 of the Centre Informatique National de l'Enseignement Supérieur (CINES, Montpellier, France), and the CRAY T3E of the RZG Computing Center (Munich, Germany), that have comparable processor speed. The number of processors and the CPU time required for the corresponding runs are also listed in Table 1.

Results have been dumped in output files for 100 time steps, equally spaced in the logarithm of the expansion factor of the Universe between $z = 20$ and $z = 0$. At each time step, a Spherical Overdensity (Lacey & Cole 1994) halo finder has been used to detect the halos, and to estimate their virial mass and radius (see Table 1). With respect to the original virial masses and radii, those of the resimulated halos show non-systematic and small differences (of the order of few percent), particularly for the most massive objects. Moreover, also the halo formation history (the way how mass assembly proceeds with time) is very similar to that in the parent simulation, thus assuring the reliability and precision of the high-resolution re-simulation technique we use. Visually, the noticeable improvement provided by such a technique

[1] Note that to get the same mass resolution ($2.07 \times 10^9 M_\odot/h$ or $10^9 M_\odot/h$) in the entire volume of the parent simulation, about 1650^3 of 2100^3 particles of would have been required.

is apparent from Figs. 1 and 2, where the images of the 3 most massive halos, before and after the resimulations, are shown at the scales of $\sim 30\,\mathrm{Mpc}/h$ and $\sim 2\,r_{\mathrm{vir}}$, respectively.

3. Observed scaling relations at $z = 0$

Analyzing a sample of 16 nearby galaxy clusters, S93 found the following relation between the observed luminosity and velocity dispersion:

$$L \propto \sigma^{1.87\pm0.44}, \tag{1}$$

where L is in units of $L_* = 1.325 \times 10^{10}\,h^{-2}L_\odot$ ($h = 1$), and σ in km/s, and between luminosity and radius:

$$L \propto R^{1.34\pm0.17}, \tag{2}$$

where R is the effective radius measured in Mpc. In both cases, the observed scatter is very large, while a considerable improvement is found when linking the three observables together in a FP-like relation. While a bi-parametric fit was performed by S93, here we derived the FP by means of the Principal Component Analysis (hereafter PCA; see e.g. Murtagh & Heck 1987), that searches for the most suitable combinations of the three observables able to describe a thin plane. By performing a PCA on the data sample of S93, we obtain the new orthogonal variables

$$p_i \equiv \alpha_i \log R + \beta_i \log L + \gamma_i \log \sigma, \tag{3}$$

with R in Mpc/h, L in $100L_*$, σ in 1000 km/s. In Fig. 3 we show the resulting distribution of the observed clusters (blue triangles) in the (p_1, p_3) and (p_1, p_2) spaces, the former providing an exact edge-on view of the FP and making apparent its small thickness.

4. Scaling relations at $z = 0$ for simulated clusters

To derive the analogous quantities for the simulated clusters, we have constructed their projected radial profiles by counting the DM particles within concentric shells around the center of mass, for three orthogonal directions. Thus, the projected half-mass radius R_{h} has been derived as the radius of the shell containing half the total number of particles, and the velocity dispersion σ has been computed by averaging the squared line of sight component of the (barycentric) velocity over all the particles within R_{h}. Since the simulated clusters, as well as the real ones, are not spherical, such a procedure gives different values of R_{h} and σ for the three considered line of sights, the maximum difference never exceeding 33% and 21% in the two cases, respectively. Finally, for converting the DM mass into light, we have adopted a mass–to–light ratio with a small dependence on the luminosity, as suggested by observations (S93; Girardi et al. 2002): $M/L \propto L^{\alpha}$, with $\alpha = 0.3$. In particular, we have assumed: $M/L = 450(M/M_0)^{\alpha/(\alpha+1)}M_\odot/L_\odot$, where $M_0 = 7.5 \times 10^{14} M_\odot$.

By performing a PCA on the 13 DM halos for the three considered lines of sights, using R_{h}, σ, and L computed as just described, we obtain a very well defined and thin FP. To check whether this FP is similar to the observed one, we have also constructed the PCA variables p_i by combining R_{h}, σ, and L derived for the DM halos, with the coefficients α_i, β_i, γ_i obtained for the observed clusters. The resulting FP is practically indistinguishable from the observed one, as apparent from Fig. 3. Moreover, also the L-σ and L-R relations of simulated and real clusters are in remarkable agreement (Fig. 4).

Note that assuming a *constant* M/L ratio, the FP of simulated clusters is still well defined, and only shows a mild tilt with respect to the observed one (see solid line in Fig. 3).

5. Scaling relations at higher redshift for simulated clusters

While no observational data are yet available for galaxy clusters at higher redshift,

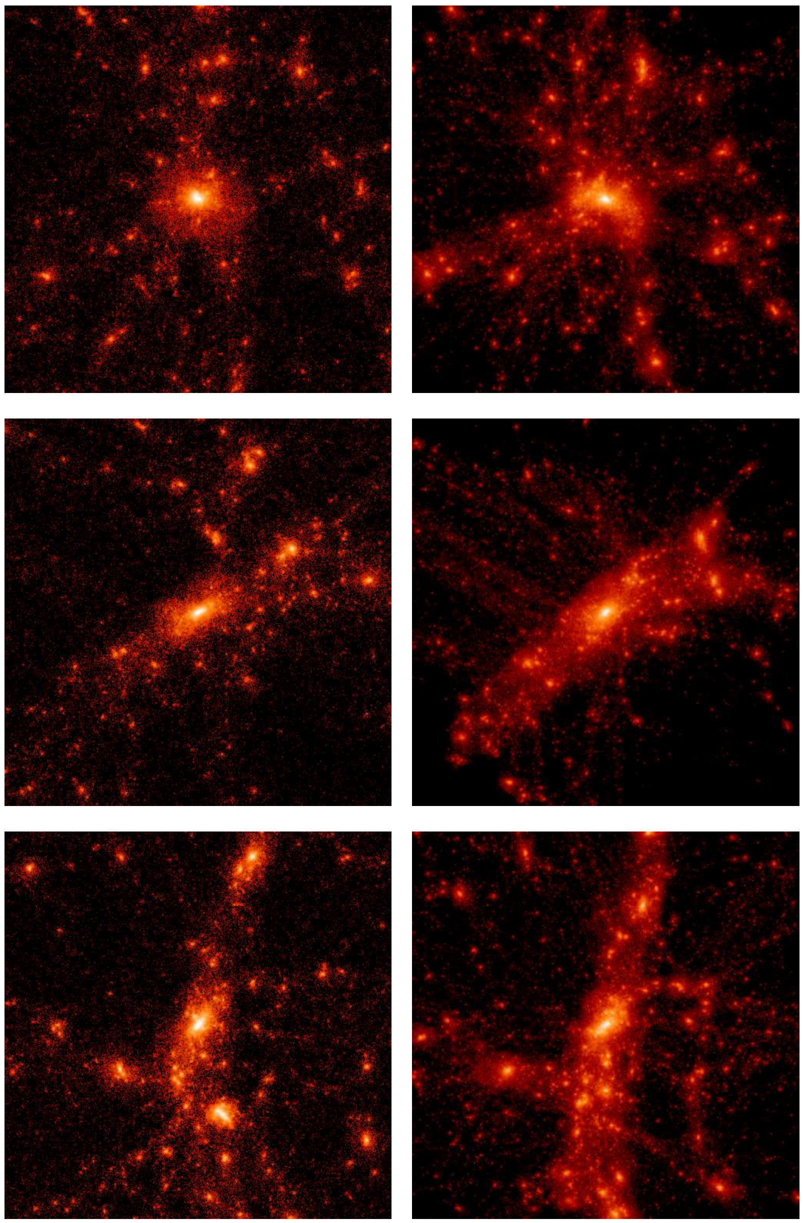

Fig. 1. Images of the 3 most massive DM halos in the parent simulation (left panels) and after the high-resolution re-simulation (right panels). All panels show the projection along an arbitrary line of sight, of a region of $\sim 30\,\mathrm{Mpc}/h$ around the halo center of mass.

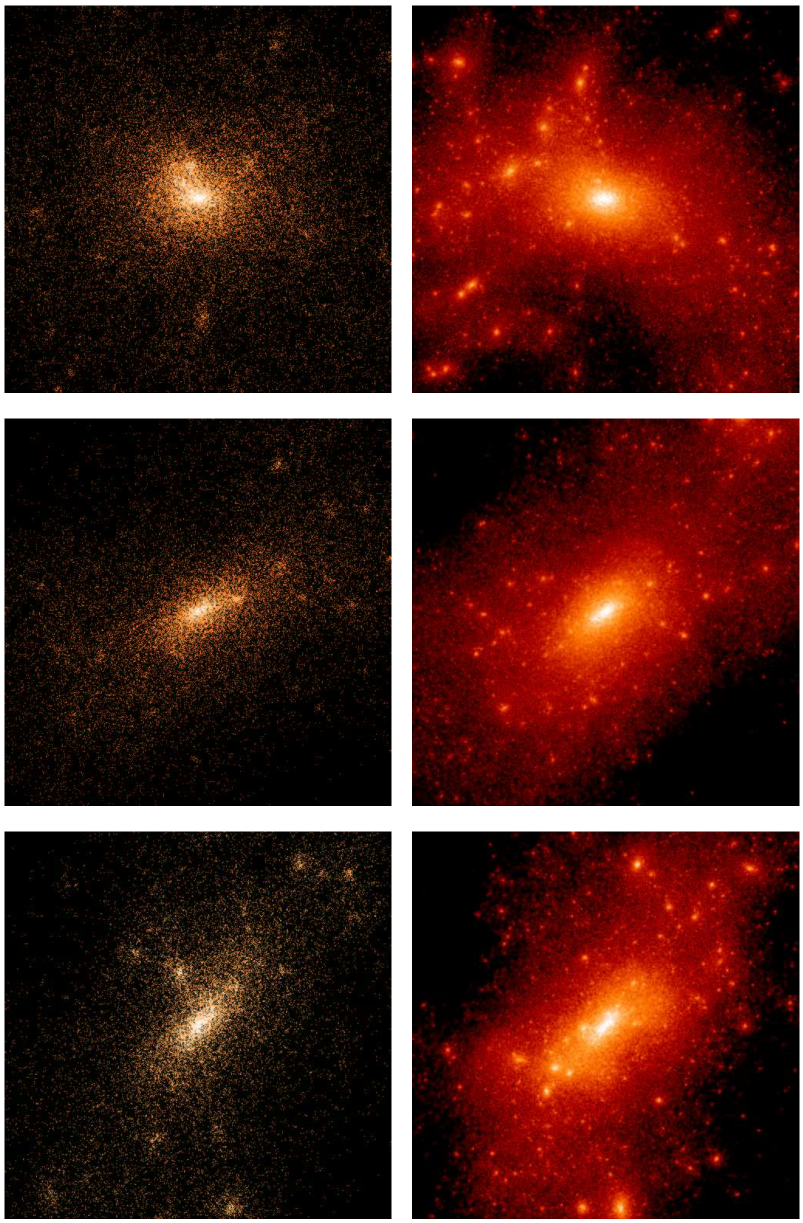

Fig. 2. Images of the 3 most massive DM halos in the parent simulation (left panels) and after the high-resolution re-simulation (right panels). All panels show the projection along an arbitrary line of sight, of a region of $\sim 2\,r_{\rm vir}$ around the halo center of mass.

Table 1. Characteristics of the high-resolution resimulations of the 13 massive halos: N_{HR} = number of high-resolution particles, N_{LR} = number of low-resolution macroparticles, N_T = total number of particles, N_{proc} = number of processors, t_{CPU} = hours per processor required for the resimulations, M_{vir} = virial mass in $10^{14} M_\odot/h$, r_{vir} = virial radius in Mpc/h.

Name	N_{HR}	N_{LR}	N_T	N_{proc}	t_{CPU}	M_{vir}	r_{vir}
g8	3700120	191733	3891853	32	80	23.42	2.75
g1	2574717	202301	2777018	32	70	13.99	2.31
g72	3299865	194277	3494142	32	57	11.77	2.18
g696	4870197	184314	5054511	64	60	11.37	2.16
g51	1677364	213477	1890841	32	44	10.78	2.12
g245	3437317	215269	3652586	16	18.4	6.50	1.79
g689	3252085	215809	3467894	16	18.3	6.08	1.75
g564	2068981	227187	2296168	16	12.8	4.91	1.63
g1777	3094123	219047	3313170	16	18.0	3.83	1.50
g4478	2293433	225706	2519139	16	12.8	2.92	1.37
g914	250605	247091	497696	16	7.3	1.45	1.09
g3344	206140	248756	454896	16	6.3	1.09	0.99
g1542	207202	248948	456150	16	6.3	0.82	0.99

our high-resolution re-simulations allow to investigate the scaling relations of their DM counterparts at any epoch. For that purpose, the most massive progenitors at $z = 0.5$ and at $z = 1$ of our 13 DM halos have been considered, and their projected half-mass radius, velocity dispersion and luminosity have been derived with the same procedure used for the $z = 0$ objects. Also in this case, when combining R_h, σ, and L with the coefficients α_i, β_i, γ_i derived for the real clusters at $z = 0$, the resulting FP is very similar to the edge-on FP observed locally, while when seen face-on, the region populated by the high-z DM halos is systematically shifted towards larger (smaller) values of p_1 (p_2) with respect to the region occupied by the observed nearby clusters. In addition, very well defined L-σ and L-R relations are already in place at these redshifts. With respect to the observed L-σ relation at $z = 0$, a flatter slope is found for increasing redshift for the simulated clusters, while the opposite trend is found in the case of the L-R relation, that becomes steeper for increasing z.

6. Discussion and conclusions

We have described a technique for increasing the (mass and spatial) resolution of objects selected in a given cosmological simulation. Applying it to sample of 13 massive halos at $z = 0$ in a ΛCDM cosmology, we have investigated whether the scaling relations observed for nearby galaxy clusters are also followed by their DM hosts, in a dissipationless hierarchical merging scenario. By considering the most massive progenitors at $z = 0.5$ and $z = 1$ of the 13 selected halos, we have also investigated whether the same scaling relations were already in place at those earlier epochs.

The main conclusions can be summarized as follows:

– the high-resolution re-simulation technique is very powerful and reliable. The precision of the method depends on the number of particles composing the original object, and on the dimension of the boundary region considered to avoid the "contamination" from macroparticles.

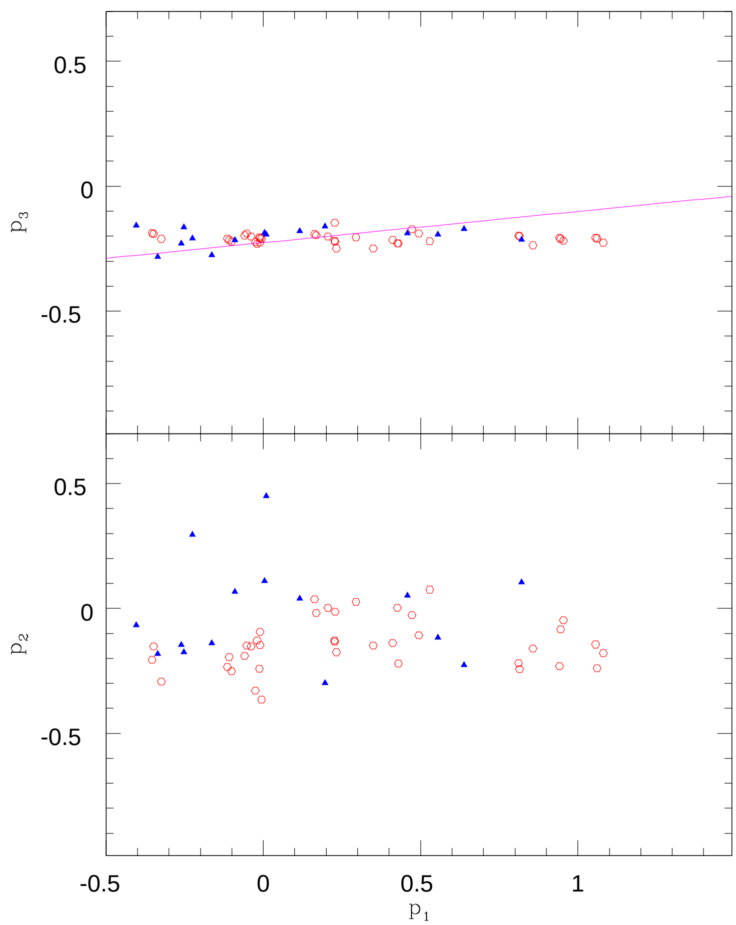

Fig. 3. Observed (blue triangles) and simulated (red hexagons) clusters in the edge-on and face-on view of the FP (upper and lower panels, respectively), at redshift $z = 0$. The linear best fit to the simulated clusters in case of a constant M/L is shown by the pink solid line.

- The DM hosts of galaxy clusters do define a FP that is practically indistinguishable from the one observed for nearby galaxy clusters.
- A very good agreement between the scaling relations of simulated and observed clusters is also found in terms of the L-σ and the L-R relations.
- The FP of simulated clusters is already defined at $z = 0.5$ and $z = 1$, and it is very similar and as thin as the one observed locally; the only differences are due to an obvious shift towards smaller radii and masses for increasing z. Also the L-σ and L-R relations are already in place at high redshifts, with a difference in the slope (with respect to the re-

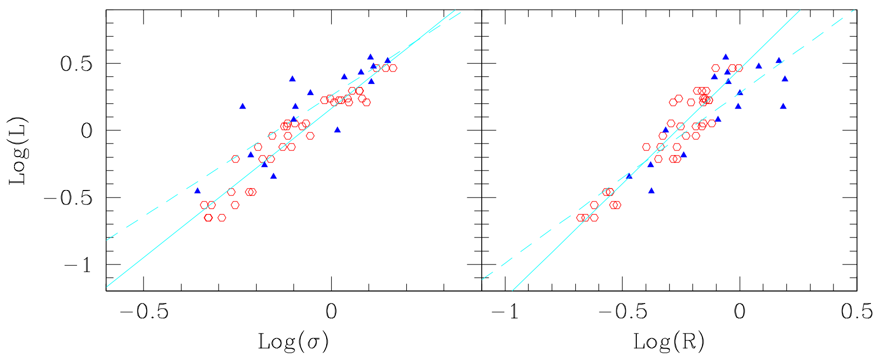

Fig. 4. L-σ (left panels) and L-R (right panels) relations for the observed (blue triangles and dashed line) and simulated (red hexagons and solid line) clusters, at redshift $z = 0$. Luminosities are in units of $100\,L_*$, velocity dispersions in km/s, and radii in Mpc.

lations observed locally) due to the fact that at recent epochs, more massive objects evolve more rapidly than smaller systems.

All the results about the scaling relations of simulated and observed clusters are obtained by assuming a mass-to-light ratio with mean value of the order of $450hM_\odot/L_\odot$ (well in agreement with what estimated from observations of galaxy clusters), and with a dependence on the luminosity also suggested by the observations.

Given the very different nature of the two components (baryonic and non baryonic) and of the physical processes acting on them, the fact that the DM halos define the same relations shown by real clusters is not obvious at all. Moreover, dissipationless hierarchical merging at galactic scales is unable to reproduce the observed scaling relations of elliptical galaxies: the end-products of major mergers do lie on the observed FP, but substantial deviations from the Faber-Jackson and the Kormendy relations are found in this case (see Londrillo et al., this conference). Such a result suggests that, while dissipation has a major role in the formation and evolution of ellipticals, it is negligible with respect to the pure gravity in settling the properties of galaxy clusters.

Acknowledgements. B.L. acknowledges G. Tormen, V. Springel, S. White, & G. Mamon for their help with the N-body simulations and for useful discussions. This work has been partially supported by the Italian Ministery (MIUR) grant COFIN2001 "Clusters and groups of galaxies: the interplay between dark and baryonic matter", and by the Italian Space Agency grants ASI-I-R-105-00 and ASI-I-I-037-01. L.C. was supported by COFIN2000.

References

Adami C., Mazure A., Biviano A., Katgert P., & Rhee G., 1998, A&A 331, 493

Beisbart C., Valdarnini R., & Buchert T., 2001, A&A 379, 412

Capelato H.V., de Carvalho R.R., & Carlberg R.G., 1995, ApJ 451, 525

Dantas C.C., Capelato H.V., Ribeiro A.L.B., & de Carvalho R.R., 2002, MNRAS accepted (astro-ph/0211251)

Djorgovski S., & Davis M. 1987, ApJ, 313, 59

Dressler A., Lynden-Bell D., Burstein D., Davies R.L., Faber S.M., Terlevich R., & Wegner G. 1987, ApJ, 313, 42

Faber S.M., & Jackson R.E. 1976, ApJ, 204, 668
Fujita Y., & Takahara F., 1999, ApJ 519, L55
Evstigneeva E.A., Reshetnikov V.P., Sotnikova N.Ya., 2002, A&A 381, 6
Girardi M., Manzato P., Mezzetti M., Giuricin G., Limboz F., 2002, ApJ 569, 720
Gonzales A.C., & van Albada T.S., 2002, MNRAS submitted
Kormendy J., 1977, ApJ 218, 333
Lacey C., & Cole S., 1994, MNRAS 271, 781
Lanzoni B., Cappi A., Ciotti L., Tormen G., & Zamorani G., in preparation
Murtagh F., Heck A., 1987, *Multivariate Data Analysis*, D.Reidel Publishing Company, Dordrecht, Holland
Nipoti C., Ciotti L., Londrillo P., 2002a, astro-ph/0112133 (NCL02a)
Nipoti C., Ciotti L., Londrillo P., 2002b, MNRAS submitted (NCL02b)
Pentericci L., Ciotti L., & Renzini A. 1995, Astrophysical Letters and Communications, 33, 213
Schaeffer R., Maurogordato S., Cappi A., Bernardeau F., 1993, MNRAS 263, L21 (S93)
Springel V., Yoshida N., & White S.D.M., 2001, New Astronomy, 6, 79
Tormen G., Bouchet F., & White S.D.M., 1997, MNRAS 286, 865
West M.J., Dekel A., Oemler A., 1987, ApJ 316, 1
Yoshida N., Sheth R.K., & Diaferio A., MNRAS 328, 669

Mem. S.A.It. Suppl. Vol. 1, 186

Memorie della
Supplementi

Elliptical galaxies interacting with the cluster tidal field: origin of the intracluster stellar population

V. Muccione[1], L. Ciotti[2]

[1] Geneva Observatory,51 ch. des Maillettes, 1290 Sauverny, Switzerland
e-mail: veruska.muccione@obs.unige.ch

[2] Dipartimento di Astronomia, Università di Bologna, via Ranzani 1, 40127 Bologna, Italy e-mail: ciotti@bo.astro.it

Abstract.
With the aid of simple numerical models, we discuss a particular aspect of the interaction between stellar orbital periods inside elliptical galaxies (Es) and the parent cluster tidal field (CTF), i.e., the possibility that *collisionless stellar evaporation* from Es is an effective mechanism for the production of the recently discovered intracluster stellar populations (ISP). These very preliminary investigations, based on idealized galaxy density profiles (such as Ferrers density distributions) show that, over an Hubble time, the amount of stars lost by a representative galaxy may sum up to the 10% of the initial galaxy mass, a fraction in interesting agreement with observational data. The effectiveness of this mechanism is due to the fact that the galaxy oscillation periods near its equilibrium configurations in the CTF are of the same order of stellar orbital times in the external galaxy regions.

Key words. Clusters: Galaxies – Galaxies: Ellipticals – Stellar Dynamics: Collisionless systems

1. Introduction

Observational evidences of an Intracluster Stellar Population (ISP) are mainly based on the identification of *intergalactic* planetary nebulae and red giant branch stars (see, e.g., Theuns & Warren 1996, Mèndez et al. 1998, Feldmeier et al. 1998, Arnaboldi et al. 2002, Durrell et al. 2002). Overall, the data suggest that approximately 10% (or even more) of the stellar mass of the cluster is contributed by the ISP (see, e.g., Ferguson & Tanvir 1998).

The usual scenario assumed to explain the finding above is that gravitational interactions between galaxies in cluster and/or interactions between the galaxies with the tidal gravitational field of the parent cluster (CTF), lead to a substantial stripping of stars from the galaxies themselves.

Here, supported by a curious coincidence, namely by the fact that *the characteristic times of oscillation of a galaxy around its equilibrium position in the CTF are of the same order of magnitude of the stellar orbital periods in the external part of the galaxy itself*, we suggest that an additional effect is at work, i.e. we discuss about the possible "resonant" interaction between stellar orbits inside the galaxies and the CTF.

In fact, based on the observational evidence that the major axis of cluster Es seems to be preferentially oriented toward the cluster center, N-body simulations showed that galaxies tend to align reacting to the CTF as rigid (Ciotti & Dutta 1994). By assuming this idealized scenario, a stability analysis then shows that this configuration is of equilibrium, and allows to calculate the oscillation periods in the linearized regime (Ciotti & Giampieri 1998, hereafter CG98).

Prompted by these observational and theoretical considerations, in our numerical explorations we assume that the galaxy is a triaxial ellipsoid with its center of mass at rest at the center of a triaxial cluster. The considerably more complicate case of a galaxy with the center of mass in rotation around the center of a spherical cluster will be discussed elsewhere (Ciotti & Muccione 2003, hereafter CM03).

2. The physical background

Without loss of generality we assume that in the (inertial) Cartesian coordinate system C centered on the cluster center, the CTF tensor $\boldsymbol{T}$ is in diagonal form, with components T_i $(i = 1, 2, 3)$. By using three successive, counterclockwise rotations (φ around x axis, ϑ around y' axis and ψ around z'' axis), the linearized equations of motion for the galaxy near the equilibrium configurations can be written as

$$\ddot{\varphi} = \frac{\Delta T_{32}\Delta I_{32}}{I_1}\varphi,$$

$$\ddot{\vartheta} = \frac{\Delta T_{31}\Delta I_{31}}{I_2}\vartheta,$$

$$\ddot{\psi} = \frac{\Delta T_{21}\Delta I_{21}}{I_3}\psi, \tag{1}$$

where ΔT is the *antisymmetric* tensor of components $\Delta T_{ij} \equiv T_i - T_j$, and I_i are the principal components of the galaxy inertia tensor. In addition, let us also assume that $T_1 \geq T_2 \geq T_3$ and $I_1 \leq I_2 \leq I_3$, i.e., that $\Delta T_{32}, \Delta T_{31}$ and ΔT_{21} are all less or equal to zero (see Section 3). Thus, the equilibrium position of 1 is *linearly stable*, and its solution is

$$\begin{aligned} \varphi &= \varphi_{\rm M}\cos(\omega_\varphi t), \\ \vartheta &= \vartheta_{\rm M}\cos(\omega_\vartheta t), \\ \psi &= \psi_{\rm M}\cos(\omega_\psi t), \end{aligned} \tag{2}$$

where

$$\begin{aligned} \omega_\varphi &= \sqrt{\frac{\Delta T_{23}\Delta I_{32}}{I_1}}, \\ \omega_\vartheta &= \sqrt{\frac{\Delta T_{13}\Delta I_{31}}{I_2}}, \\ \omega_\psi &= \sqrt{\frac{\Delta T_{12}\Delta I_{21}}{I_3}}. \end{aligned} \tag{3}$$

For computational reasons the best reference system in which calculate stellar orbits is the (non inertial) reference system C' in which the galaxy is at rest, and its inertia tensor is in diagonal form. The equation of the motion for a star in C' is

$$\ddot{\boldsymbol{x}}' = \mathcal{R}^{\rm T}\ddot{\boldsymbol{x}} - 2\boldsymbol{\Omega}\wedge\boldsymbol{v}' - \dot{\boldsymbol{\Omega}}\wedge\boldsymbol{x}' - \boldsymbol{\Omega}\wedge(\boldsymbol{\Omega}\wedge\boldsymbol{x}'), \tag{4}$$

where $\boldsymbol{x} = \mathcal{R}(\varphi, \vartheta, \psi)\boldsymbol{x}'$, and

$$\begin{aligned} \boldsymbol{\Omega} \; = \; & (\dot{\varphi}\cos\vartheta\cos\psi + \dot{\vartheta}\sin\psi, -\dot{\varphi}\cos\vartheta\sin\psi \\ & +\dot{\vartheta}\cos\psi, \dot{\varphi}\sin\vartheta + \dot{\psi}). \end{aligned} \tag{5}$$

In eq. (4)

$$\mathcal{R}^{\rm T}\ddot{\boldsymbol{x}} = -\nabla_{\boldsymbol{x}'}\phi_{\rm g} + (\mathcal{R}^{\rm T}\boldsymbol{T}\mathcal{R})\boldsymbol{x}', \tag{6}$$

where $\phi_{\rm g}(\boldsymbol{x}')$ is the galactic gravitational potential, $\nabla_{\boldsymbol{x}'}$ is the gradient operator in C', and we used the tidal approximation to obtain the star acceleration due to the cluster gravitational field.

3. Period estimations

For simplicity, in the following estimates we assume that the galaxy and cluster densities are stratified on homeoids. In particular, we use a galaxy density profile belongings to the ellipsoidal generalization of the widely used γ-models (Dehnen 1993, Tremaine et al. 1994):

$$\rho_{\rm g}(m) = \frac{M_{\rm g}}{\alpha_1\alpha_2\alpha_3}\frac{3-\gamma}{4\pi}\frac{1}{m^\gamma(1+m)^{4-\gamma}}, \quad (7)$$

where $M_{\rm g}$ is the total mass of the galaxy, $0 \leq \gamma \leq 3$, and

$$m^2 = \sum_{i=1}^{3}\frac{(x_i')^2}{\alpha_i^2}, \qquad \alpha_1 \geq \alpha_2 \geq \alpha_3. \quad (8)$$

The inertia tensor components for this family are given by

$$I_i = \frac{4\pi}{3}\alpha_1\alpha_2\alpha_3(\alpha_j^2+\alpha_k^2)h_{\rm g}, \quad (9)$$

where $h_{\rm g} = \int_0^\infty \rho_{\rm g}(m)m^4 dm$, and so $I_1 \leq I_2 \leq I_3$. Note that, from eq. (3), *the frequencies for homeoidal stratifications do not depend on the specific density distribution assumed, but only on the quantities* $(\alpha_1, \alpha_2, \alpha_3)$. We also introduce the two ellipticities

$$\frac{\alpha_2}{\alpha_1} \equiv 1-\epsilon, \qquad \frac{\alpha_3}{\alpha_1} \equiv 1-\eta, \quad (10)$$

where $\epsilon \leq \eta \leq 0.7$ in order to reproduce realistic flattenings.

A rough estimate of *characteristic stellar orbital times* inside m is given by $P_{orb}(m) \simeq 4P_{dyn}(m) = \sqrt{3\pi/G\overline{\rho_{\rm g}}(m)}$, where $\overline{\rho_{\rm g}}(m)$ is the mean galaxy density inside m. We thus obtain

$$P_{orb}(m) \simeq 9.35\times 10^6\sqrt{\frac{\alpha_{1,1}^3(1-\epsilon)(1-\eta)}{M_{\rm g,11}}} \times m^{\gamma/2}(1+m)^{(3-\gamma)/2}\ \text{yrs}, \quad (11)$$

where $M_{\rm g,11}$ is the galaxy mass normalized to $10^{11}M_\odot$, $\alpha_{1,1}$ is the galaxy "core" major axis in kpc units (for the spherically symmetric $\gamma = 1$ Hernquist 1990 models, $R_{\rm e} \simeq 1.8\alpha_1$); thus, in the outskirts of normal galaxies orbital times well exceeds 10^8 or even 10^9 yrs.

For the cluster density profile we assume

$$\rho_{\rm c}(m) = \frac{\rho_{\rm c,0}}{(1+m^2)^2}, \quad (12)$$

where m is given by an identity similar to eq. (8), with $a_1 \geq a_2 \geq a_3$, and, in analogy with eq. (10), we define $a_2/a_1 \equiv 1-\mu$ and $a_3/a_1 \equiv 1-\nu$, with $\mu \leq \nu \leq 1$.

It can be shown that the CTF components at the center of a non-singular homeoidal distribution are given by

$$T_i = -2\pi G\rho_{\rm c,0}w_i(\mu,\nu), \quad (13)$$

where the dimensionless quantities w_i are independent of the specific density profile, $w_1 \leq w_2 \leq w_3$ for $a_1 \geq a_2 \geq a_3$, and so the conditions for stable equilibrium in eq. (1) are fulfilled (CG98, CM03).

The quantity $\rho_{\rm c,0}$ is not a well measured quantity in real clusters, and for its determination we use the virial theorem, $M_{\rm c}\sigma_{\rm V}^2 = -U$, where $\sigma_{\rm V}^2$ is the virial velocity dispersion, that we assume to be estimated by the observed velocity dispersion of galaxies in the cluster. Thus, we can now compare the galactic oscillation periods (for small galaxy and cluster flattenings, see CM03)

$$\begin{aligned} P_\varphi &= \frac{2\pi}{\omega_\varphi} \simeq \frac{8.58\times 10^8}{\sqrt{(\nu-\mu)(\eta-\varepsilon)}}\frac{a_{1,250}}{\sigma_{\rm V,1000}}\ \text{yrs}, \\ P_\vartheta &= \frac{2\pi}{\omega_\vartheta} \simeq \frac{8.58\times 10^8}{\sqrt{\nu\eta}}\frac{a_{1,250}}{\sigma_{\rm V,1000}}\ \text{yrs}, \\ P_\psi &= \frac{2\pi}{\omega_\psi} \simeq \frac{8.58\times 10^8}{\sqrt{\mu\varepsilon}}\frac{a_{1,250}}{\sigma_{\rm V,1000}}\ \text{yrs}. \end{aligned} \quad (14)$$

(where $a_{1,250} = a_1/250$kpc, and $\sigma_{\rm V,1000} = \sigma_{\rm V}/10^3$km s^{-1}) with the characteristic orbital times in galaxies. From eqs. (11) and (14), it follows that *in the outer halo of giant Es the stellar orbital times can be of the same order of magnitude as the oscillatory periods of the galaxies themselves in the CTF*. For example, in a relatively small galaxy of $M_{\rm g,11} = 0.1$ and $\alpha_{1,1} = 1$,

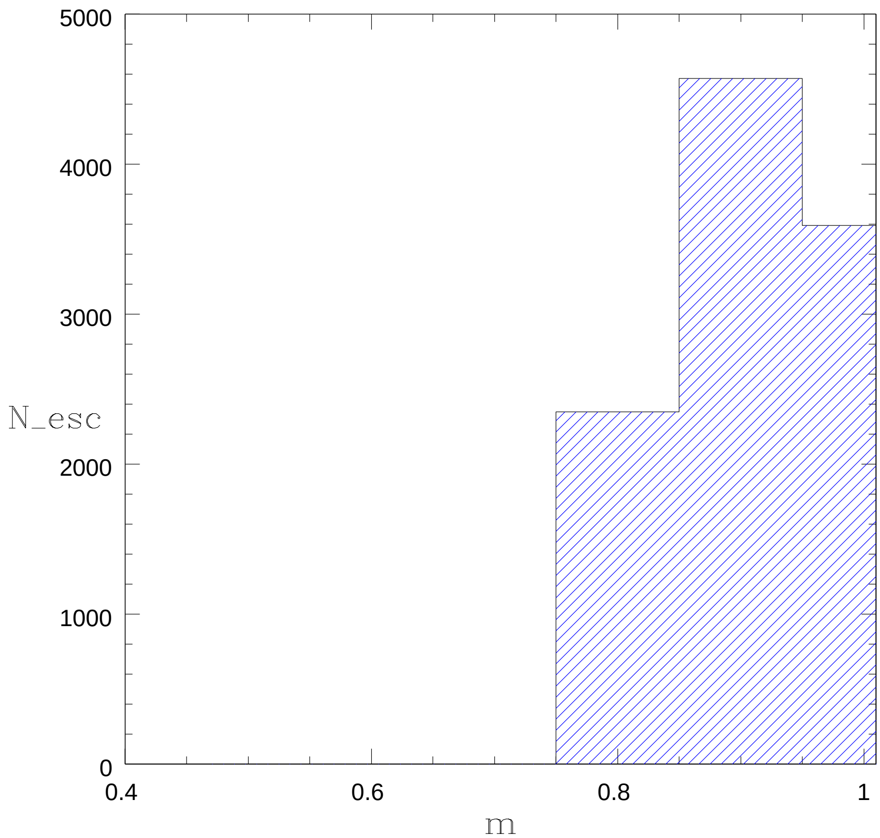

Fig. 1. Histogram of m at $t = 0$ vs. $N_{\rm esc}$ for a galaxy of $M_{\rm g} = 10^{10}\, M_{\odot}$ and $\alpha_1 = 20$ kpc, with $\epsilon = 0.2$ and $\eta = 0.4$. The cluster parameters are $\mu = 0.2$, $\nu = 0.4$, $a_{1,250} = \sigma_{\rm V,1000} = 1$, and the galaxy maximum oscillations angles in eqs. (2) are fixed to 0.2 rad. In this simulation $N_{\rm tot} = 10^5$.

$P_{orb} \simeq 1$ Gyr is at $m \simeq 10$ (i.e., at $\simeq 5R_{\rm e}$), while for a galaxy with $M_{\rm g,11} = 1$ and $\alpha_{1,1} = 3$ the same orbital time is at $m \simeq 7$ (i.e., at $\simeq 3.5R_{\rm e}$).

4. The numerical integration scheme

Here we present the preliminary results obtained by using only a very idealized galactic density profile, while more realistic galaxy density distributions, such as triaxial Hernquist models, are described elsewhere (CM03, Muccione & Ciotti 2003, hereafter MC03). In particular, here we explore the evaporation process in the case of a Ferrers (see, e.g., Binney & Tremaine

1987) models, with density profiles given by

$$\rho_g = \begin{cases} \rho_g(0)(1-m^2)^n & \text{for } m \leq 1 \\ 0 & \text{for } m > 1 \end{cases} \quad (15)$$

where m is the homeoidal radius defined as in eq. (8). The case $n = 0$ corresponds to an anisotropic harmonic oscillator, while for $n \geq 0$ the density distribution is radially decreasing. A nice property of Ferrers models (for integer n) is that their gravitational potential can be simply expressed in algebraic form (see, e.g., Chandrasekhar 1969).

To integrate the second order differential equations (11) for each star, we use a code based on an adapted Runge-Kutta routine. The initial conditions are obtained by using the Von Neumann *rejection method*, and with this method we arrange $N_{\rm tot}$ initial conditions in configuration space which reproduce the density profile in eq. (15). In MC03 and CM03 the three components of the initial velocity for each star are assigned by considering the local velocity dispersion of the galaxy model at rest, while here, for simplicity, each star at $t = 0$ is characterized by null velocity. Within $t = t_{\rm H}$ (where $t_{\rm H} = 1.5 \times 10^{10}$ yrs), the code checks which of the initial conditions result in a orbit with $m > 1$. This escape condition is very crude, and a more sophisticated criterium is adopted in MC03 and CM03, where *untruncated* galaxy models are used. In standard simulations we use, as a rule, $N_{\rm tot} = 10^5$, thus, from this point of view, we are exploring 10^5 independent "1-body problems" in a time–dependent force field.

The simulations are performed on the *GRAVITOR*, the Geneva Observatory 132 processors Beowulf cluster (**http://obswww.unige.ch/~pfennige/gravitor/gravitor_e.html**).

5. Preliminary results and conclusions

In Fig. 1 we show the results of one of our preliminary simulations for a galaxy model with $n = 1$, $M_{\rm g} = 10^{10} M_{\odot}$, semi-mayor axis $\alpha_1 = 20$ kpc, flattenings $\epsilon = 0.2$, $\eta = 0.4$, and maximum oscillation angles equals to 0.2 rad. The cluster parameters are $a_{1,250} = \sigma_{\rm V,1000} = 1$, $\mu = 0.2$, $\nu = 0.4$, and the total number of explored orbits is $N_{\rm tot} = 10^5$. In the ordinate axis we plot the number of *escapers* as a function of their homeoidal radius at $t = 0$. Note how the zone of maximum escape is near $m \simeq 0.8$, and how the total number of escapers is a significant fraction of the total number of explored orbits (actually, with the galaxy and cluster parameters adopted in the simulations, $N_{\rm esc} \simeq 0.1 N_{\rm tot}$). This number is a somewhat upper limit of the expected number in more realistic simulations: in fact, 1) as described in Section 4, we adopted a very weak escape criterium, and 2), in more realistic galaxy models the density decrease in the outer parts is stronger than in Ferrers models, and so we expect that a smaller number of stars will be significantly affected by the CTF. Both points are addressed and discussed elsewhere, in MC03 in a preliminary and qualitative way for an Hernquist model at the center of a cluster, while in CM03 we present the results of a systematic exploration of the parameter space for untruncated galaxies both at the center and with the center of mass in circular orbit in a spherical cluster.

In any case, the simple model here explored looks promising, with a number of escapers in nice agreement with the observational estimates.

Acknowledgements. We would like to thank Giuseppe Bertin and Daniel Pfenniger for useful discussions and the Observatory of Geneve which has let us use the GRAVITOR for our simulations. L.C. was supported by the grant CoFin2000.

References

Arnaboldi M., Aguerri J.A.L., Napolitano N.R., Gerhard O., Freeman K.C., Feldmeier J., Capaccioli M., Kudritzki R.P., Méndez R.H., 2002, AJ 123, 760

Binney J., Tremaine S., 1987, Galactic Dynamics, Princeton University Press (Princeton)
Chandrasekhar S., 1969, Ellipsoidal Figures of Equilibrium, Dover (New York)
Ciotti L., Dutta S.N., 1994, MNRAS 270, 390
Ciotti L., Giampieri G., 1998, Cel.Mech. & Dyn.Astr. 68, 313 (CG98)
Ciotti L., Muccione V., 2003, in preparation (CM03)
Dehnen W., 1993, MNRAS 256, 250
Durrell P.R. et al. 2002, ApJ 570, 119
Feldmeier J.J., Ciardullo R., Jacoby G.H., 1998, ApJ 503, 109
Ferguson H.C., Tanvir N.R., von Hippel T., 1998, Nature 391, 461
Hernquist, L., 1990, ApJ 356, 359
Méndez R.H. et al, 1998, ApJ 491, L23
Muccione V., Ciotti L., 2003, Galaxies and Chaos, G. Contopoulos & N. Voglis, eds., Springer-Verlag, in press (MC03)
Theuns T., Warren S.J., 1996, MNRAS 284, L11
Tremaine S. et al., 1994, AJ 107, 634